

Spin transfer and current-induced switching in antiferromagnets

Helen V. Gomonay

National Technical University of Ukraine “KPI”
ave Peremogy, 37, 03056, Kyiv, Ukraine

Vadim M. Loktev

Bogolyubov Institute for Theoretical Physics NAS of Ukraine,
Metrologichna str. 14-b, 03143, Kyiv, Ukraine

(Dated: October 30, 2018)

Recent experiments show that spin-polarized current may influence the state of generally accessory element of spin-valves – an antiferromagnetic (AFM) layer, which is used for “pinning”. Here we study the dynamics of AFM component of the “pinned” ferromagnetic (FM) layer induced by simultaneous application of the spin-polarized current and external magnetic field.

We find stability range of such a configuration of FM/AFM system in which orientation of FM magnetization is parallel to AFM vector. We calculate the field dependence of the critical current for different orientations of the external magnetic field with respect to the crystal axes of FM/AFM bilayer. We show the possibility of stable current-induced precession of AFM vector around FM magnetization with the frequency that linearly depends on the bias current. Furthermore, we estimate an optimal duration of the current pulse required for switching between different states of FM/AFM system and calculate the current and field dependencies of switching time. The results obtained reveal the difference between dynamics of ferro- and antiferromagnets subjected to spin transfer torques.

PACS numbers: 72.25.-b, 72.25.Mk, 75.50.Ee

Keywords: Spin transfer torque, spin-polarized current, antiferromagnet

I. INTRODUCTION

Spin transfer torque (STT) is the torque that is applied by non-equilibrium spin-polarized conduction electrons onto a magnetic layer¹⁻³. This effect creates, for example, the ability to switch nanoscale magnetic devices at GHz frequencies and stimulate emission of microwaves by steady electric current^{4,5}. Key elements of the spintronic devices, that enable an information coding, control and manipulation by an electric current, are two ferromagnetic (FM) layers. The “pinned” layer acts as a polarizer for conduction electrons, while the state of a “free” layer may be altered by STT. However, recent experiments⁶⁻¹⁰ give an indirect evidence that the spin-polarized current may also influence the state of another, generally accessory, element – an antiferromagnetic (AFM) layer, which is used for “pinning”.

The characteristic value of current density at which the switching of AFM state takes place varies from 10^5 A/cm² (for an insulating AFM and current-in-plane geometry⁹) to 10^8 A/cm² (for a metallic AFM and current-perpendicular-to-plane geometry⁶) and, in principle, can be smaller than the critical current density in the similar giant magnetoresistive structures without an AFM layer ($\propto 10^7 \div 10^9$ A/cm², Refs.11–13). Spin-polarized current also affects both the exchange bias and the coercive field of “free” FM layer¹⁴. Combined application of spin-polarized current and external magnetic field gives rise to various switching scenarios depending on the thickness, sequence and material of FM and AFM layers¹⁴. On the other hand, the physical mechanism and details of such a nontrivial dynamics are still unclear.

Due to the efforts of several theoretical groups¹⁵⁻¹⁸ the concept of STT is extended to the systems with *i*) different types of magnetic ordering, including nonuniform and disordered FM (that, in principle, could be further extended to the magnetic systems with noncollinear and, probably, AFM spin ordering); *ii*) different nature of the magnetic ordering and interaction between the charge carriers and spins, i.e., *sd*-exchange in the magnets with localized spins or itinerant magnetism in the transition metals. It also became clear that the STT phenomena could result from the atomic scale spin dependent scattering (i.e., hopping of a conduction electron between the sites with different directions of the magnetic moments). In some particular cases an AFM can even work as a polarizer for conduction electrons and exert spin torque on the adjacent FM or AFM layer, as it was predicted in Refs.16 and 17. However, all of the published calculations are based on assumption of quantum coherence and so, are applicable to the perfect samples with ideal interfaces.

In our previous paper¹⁹ we proposed the phenomenological model that describes the current-induced phenomena in AFMs on the same footing as in FM materials. It was assumed that the total angular momentum is conserved during an interaction of spin-polarized transport electrons with each of magnetic sublattices.

In the present paper we apply this model for the description of the precessional switching processes induced by simultaneous application of the spin-polarized current and external magnetic field to an AFM component of the “pinned” layer depicted in Fig. 1(a). Our chief aim is to study the different static and dynamic regimes of AFM

layer and to find the way to induce a stable precession of an AFM vector starting from a certain configuration of FM/AFM bilayer. We also try to find similar and different features in the current-induced dynamics of FM/FM and FM/AFM bilayers. We anticipate our approach to be a starting point for a more comprehensive analysis of the multilayered magnetic systems in the presence of high-density current. For example, joint behavior of the FM and AFM layers could be analyzed, with account of the exchange bias coupling.

II. SPIN TRANSFER TORQUE IN THE MULTISUBLATTICE MAGNETS

According to Berger¹ and Slonczewski^{2,3}, the physical mechanism of STT in ferromagnets can be explained in the following way. When a free electron transverses (or reflects from) an interface between the nonmagnetic (NM) and FM layers, its spin state can be reversed due to exchange interaction with the localized magnetic moments of FM. This process results in rotation of the localized moments in a way that ensures conservation of the total spin of the system.

Generalization of the Berger's and Slonczewski's ideas to the case of multisublattice materials is not straightforward due to more complex character of the magnetic ordering. Particularly, in AFMs the direction of the atomic magnetic moments varies on the length scale of atomic distances leading to zero net magnetization if averaged over few lattice constants. However, just as in FMs, the spin-polarized electrons transfer spin torques on each of atomic sites^{16,18,20,21}.

The magnetic structure of AFM may be described with the use of a few macroscopic vectors \mathbf{M}_j (in the simplest case $j = 1, 2$) called the sublattice magnetizations (per unit volume) that are formed due to strong exchange coupling. So, it seems reasonable to assume that while entering an AFM, the conduction electron transfers spin angular momentum to any of the magnetic sublattices (see Fig. 1b). Corresponding STT \mathbf{T}_j exerted by the j -th sublattice is then presented in a standard form as follows:

$$\mathbf{T}_j = \frac{\sigma_j J}{M_{0j}} [\mathbf{M}_j \times [\mathbf{M}_j \times \mathbf{p}_{\text{cur}}]], \quad (1)$$

where J is the current spin-polarized in \mathbf{p}_{cur} direction, $|\mathbf{p}_{\text{cur}}| = 1$, the constant $\sigma_j = \varepsilon \hbar \gamma / (2M_{0j} V e)$ is proportional to the efficiency ε of scattering processes, V is the volume of AFM region, \hbar is the Plank constant, e is the electron charge, γ is the modulus of the gyromagnetic ratio, and $M_{0j} = |\mathbf{M}_j|$ is the saturation magnetization of j -th sublattice (the value of M_{0j} is supposed to be unchanged under external fields). Positive current ($J > 0$) corresponds to injection of electrons into AFM layer.

Then, the dynamics of AFM can be described by a set of Landau-Lifshitz-Gilbert equations for \mathbf{M}_j vectors

supplemented with the Slonczewski term (1):

$$\begin{aligned} \dot{\mathbf{M}}_j = & -\gamma [\mathbf{M}_j \times \mathbf{H}_j] + \frac{\alpha_G}{M_{0j}} [\mathbf{M}_j \times \dot{\mathbf{M}}_j] \\ & + \frac{\sigma_j J}{M_{0j}} [\mathbf{M}_j \times [\mathbf{M}_j \times \mathbf{p}_{\text{cur}}]], \end{aligned} \quad (2)$$

where $\mathbf{H}_j \equiv -\partial w / \partial \mathbf{M}_j$ is the "generalized force" (an effective local field acting on the magnetic moment of a sublattice) and w is free energy (per unit volume) of an AFM layer. For the sake of clarity we describe relaxation of an AFM layer in the simplest form, with the use of a single Gilbert damping parameter α_G equal for all magnetic sublattices (although the relaxation mechanisms in AFM crystals are very complicated and diverse²².)

The last two terms in r.h.s. of Eq. (2) are responsible for dissipation processes in the AFM layer. To illustrate this fact we calculate the rate of free energy losses in assumption that dissipation is small and in zero approximation $\dot{\mathbf{M}}_j = -\gamma [\mathbf{M}_j \times \mathbf{H}_j]$. Thus,

$$\begin{aligned} \frac{dw}{dt} = & - \sum_j \left(\mathbf{H}_j \cdot \dot{\mathbf{M}}_j \right) \\ = & - \sum_j \left[\frac{\alpha_G}{\gamma M_{0j}} \dot{\mathbf{M}}_j^2 - \frac{\sigma_j J}{\gamma M_{0j}} \left(\mathbf{p}_{\text{cur}} \cdot [\mathbf{M}_j \times \dot{\mathbf{M}}_j] \right) \right]. \end{aligned} \quad (3)$$

In principle, Eqs. (2), (3) could be used for description of different complicated magnetic structures (compensated AFMs, weak FMs, ferrimagnets). In the limiting case of the completely equivalent sublattices ($\mathbf{M}_1 = \mathbf{M}_2 = \dots$) the set of equations (2) turns into a standard Landau-Lifshitz-Gilbert-Slonczewski equation for FMs.

In the particular case of AFM with two magnetic sublattices it is more suitable to rewrite Eqs. (2) in terms of macroscopic magnetization (FM vector) $\mathbf{m} \equiv \mathbf{M}_1 + \mathbf{M}_2$ and AFM order parameter (AFM vector) $\mathbf{l} \equiv \mathbf{M}_1 - \mathbf{M}_2$:

$$\begin{aligned} \dot{\mathbf{m}} = & \gamma \left([\mathbf{H}_M \times \mathbf{m}] + [\mathbf{H}_L \times \mathbf{l}] \right) + \frac{\alpha_G}{2M_0} \left([\mathbf{m} \times \dot{\mathbf{m}}] + [\mathbf{l} \times \dot{\mathbf{l}}] \right) \\ & + \frac{\sigma J}{2M_0} \left([\mathbf{m} \times [\mathbf{m} \times \mathbf{p}_{\text{cur}}]] + [\mathbf{l} \times [\mathbf{l} \times \mathbf{p}_{\text{cur}}]] \right) \end{aligned} \quad (4)$$

$$\begin{aligned} \dot{\mathbf{l}} = & \gamma \left([\mathbf{H}_M \times \mathbf{l}] + [\mathbf{H}_L \times \mathbf{m}] \right) + \frac{\alpha_G}{2M_0} \left([\mathbf{m} \times \dot{\mathbf{l}}] + [\mathbf{l} \times \dot{\mathbf{m}}] \right) \\ & + \frac{\sigma J}{2M_0} \left([\mathbf{m} \times [\mathbf{l} \times \mathbf{p}_{\text{cur}}]] + [\mathbf{l} \times [\mathbf{m} \times \mathbf{p}_{\text{cur}}]] \right) \end{aligned} \quad (5)$$

Here $\mathbf{H}_M = -\partial w / \partial \mathbf{m}$ is an effective magnetic field within an AFM layer that includes an external magnetic field, $\mathbf{H}_L = -\partial w / \partial \mathbf{l}$ is a magnetic anisotropy field conjugated to an AFM order parameter, and $|\mathbf{M}_1| = |\mathbf{M}_2| = M_0$.

Equations (4), (5) describe the dynamics of FM and AFM vectors in the presence of spin-polarized current and generalize the Landau-Lifshitz-Gilbert-Slonczewski equation for the systems with more than one magnetic sublattice. In what follows we base our considerations on these equations.

III. MODEL

Let us consider a pinned layer (Fig. 1a) of a typical exchange-bias spin-valve that includes an AFM layer whose thickness d_{AFM} is much smaller than the characteristic scale of the magnetic inhomogeneity. On the other hand, d_{AFM} is large enough to ensure an AFM ordering within the layer. High current densities are achieved in a small region (10÷100 nm in diameter), in which both FM and AFM layers could be considered as a single domain. In the case of a moderate pinning (i.e., when the magnetic anisotropy of FM is comparable with the unidirectional anisotropy induced by exchange bias) the FM works as a spin-polarizer whose state is not affected by the precession of AFM vector in the adjacent layer. So, magnetization of the FM layer is assumed to be fixed and is described by the vector \mathbf{p}_{cur} .

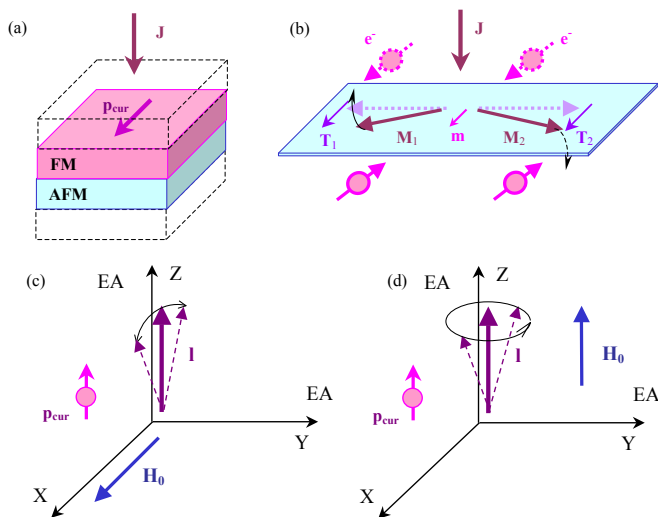


Figure 1. (Color online) **Effect of spin transfer torque within a pinned layer.** (a) General structure of a pinned layer. Due to exchange coupling, an AFM layer pins the direction of magnetization \mathbf{p}_{cur} of the adjacent FM layer. In turns, the FM layer polarizes the spin current flowing to AFM. (b) Transfer of spin torques $\mathbf{T}_{1,2}$ from free electrons (e^-) to sublattice magnetizations \mathbf{M}_1 and \mathbf{M}_2 (solid arrows – before and dotted arrows – after an interaction with the conduction electrons). STT produces small FM moment \mathbf{m} which, in turn, sets up a solid-like rotation of \mathbf{M}_1 , \mathbf{M}_2 around \mathbf{m} (arc arrows), according to Eq. (6). (c), (d) Sketch of eigen modes of an AFM vector for different orientations of the external magnetic field. Easy axes (EA) are parallel to the film plane.

In our analysis we take into account the fact that AFMs (e.g., FeMn, IrMn) widely used in spintronic devices show strong exchange coupling (corresponding exchange field $H_E \gg H_L$) between the different magnetic

sublattices that keeps magnetizations \mathbf{M}_1 and \mathbf{M}_2 almost antiparallel even in the presence of the external field $H_0 \ll H_E$. In this case the state of AFM is described by the only vector order parameter \mathbf{l} , and far below the Néel temperature $|\mathbf{l}| \approx 2M_0$. Spin-polarized current and/or external magnetic field induce small tilt of the sublattice magnetizations (Fig. 1b) formally described by the FM vector \mathbf{m} . Vector $|\mathbf{m}| \ll |\mathbf{l}|$ is a slave variable and can be expressed from Eq. (5) as follows (see Appendix A for details):

$$\mathbf{m} = \frac{[\dot{\mathbf{l}} \times \mathbf{l}]}{2\gamma M_0 H_E} + \frac{1}{2M_0 H_E} [\mathbf{l} \times [\mathbf{H}_0 \times \mathbf{l}]], \quad (6)$$

where \mathbf{H}_0 is the external magnetic field (which, particularly, can be induced by Oersted field of a current).

Substitution of the expression (6) into Eq. (4) gives rise to a closed equation for AFM vector:

$$\begin{aligned} [\ddot{\mathbf{l}} \times \mathbf{l}] = \gamma \left\{ \right. & \left(2\dot{\mathbf{l}}(\mathbf{H}_0, \mathbf{l}) - [\mathbf{l} \times [\dot{\mathbf{H}}_0 \times \mathbf{l}]] \right) \\ & - \gamma [\mathbf{H}_0 \times \mathbf{l}](\mathbf{H}_0, \mathbf{l}) + 2\gamma M_0 H_E [\mathbf{H}_L \times \mathbf{l}] \\ & \left. + \alpha_G H_E [\mathbf{l} \times \dot{\mathbf{l}}] + \sigma J H_E [\mathbf{l} \times [\mathbf{l} \times \mathbf{p}_{\text{cur}}]] \right\}. \quad (7) \end{aligned}$$

Equation (7) describes a solid-like motion of AFM vector in which $|\mathbf{l}|$ is almost unchanged. Nevertheless, due to additional (compared to FM) degrees of freedom, this equation differs from the standard Landau-Lifshitz-Gilbert-Slonczewski equation for FM vector \mathbf{M} (see (2) for $j=1$) in order (includes the 2-nd order derivative of the dynamic variable, $\ddot{\mathbf{l}}$ instead of $\dot{\mathbf{M}}$).

Analysis of the last term in (7) shows that the current-induced contribution is proportional to the AFM order parameter (vector \mathbf{l}). Thus, one can expect the influence of spin-polarized current on the dynamics of AFM vector to be at least as strong as in FM materials (other things being equal). Moreover, the current-dependent (STT) term in the r.h.s. of Eq. (7) contains large multiplier H_E . This is manifestation of the so-called effect of exchange enhancement when some interactions (e.g., gap values, spin-phonon coupling) are more pronounced in AFMs than the analogous interactions in FMs²³.

IV. DYNAMICS OF AFM VECTOR WITHIN THE LAGRANGE APPROACH

An effective formalism for investigation of AFM dynamics is based on the use of Lagrange formalism²⁴. Equation (7) can be regarded as an Euler-Lagrange equation of the second kind in the presence of dissipative external forces (see Appendix B). Corresponding Lagrange function has a form

$$\mathcal{L}_{\text{AFM}} = \frac{1}{4\gamma^2 M_0 H_E} \dot{\mathbf{l}}^2 - \frac{1}{2\gamma M_0 H_E} (\mathbf{H}_0 \cdot [\mathbf{l} \times \dot{\mathbf{l}}]) + \frac{1}{4M_0 H_E} [\mathbf{l} \times \mathbf{H}_0]^2 - w_{\text{an}}(\mathbf{l}). \quad (8)$$

Here $w_{an}(\mathbf{l})$ is the energy of magnetic anisotropy (per unit volume).

To take into account the effect of STT that can work both as a source or drain of energy for an AFM layer, we deduce from (3) the dissipative Rayleigh function (see Appendix B)

$$\mathcal{R}_{AFM} = \frac{\alpha_G}{4\gamma M_0} \dot{\mathbf{l}}^2 - \frac{\sigma J}{2\gamma M_0} (\mathbf{p}_{cur} \cdot [\mathbf{l} \times \dot{\mathbf{l}}]) \quad (9)$$

that describes the rate of the energy losses

$$\frac{dw}{dt} \equiv -\dot{\mathbf{l}} \cdot \left(\frac{\partial \mathcal{R}_{AFM}}{\partial \dot{\mathbf{l}}} \right). \quad (10)$$

Analysis of dissipative function (9) shows that STT phenomena in AFM have one general property which is not peculiar to FM. While STT always changes the energy of FM layer, some types of motions in AFM could be nondissipative even in the presence of spin-polarized current. Linearly polarized oscillations of the vector \mathbf{l} , sketched in Fig. 1c, give an example of nondissipative mode (neglecting the internal damping). And, vice versa, the most effective energy pumping induced by the current takes place for any precessional, circular polarized motion of AFM vector in the plane perpendicular to the direction of current polarization \mathbf{p}_{cur} (see Fig. 1d).

V. STABILITY DIAGRAM

To illustrate the peculiarities of non-dissipative and dissipative current-induced dynamics, we analyze stability of the state with parallel orientation of AFM and FM vectors, $\mathbf{p}_{cur} \parallel \mathbf{l}$, for two different configurations of the external magnetic field \mathbf{H}_0 , depicted schematically in Figs. 1c,d. For the definiteness, an AFM layer is supposed to have slightly tetragonal (almost cubic) anisotropy induced, e.g., by the shape effects or/and interaction with the neighboring layers (including possible influence of the exchange bias). Two easy axes (Z and Y) are parallel to the film plane. In this case the magnetic anisotropy energy w_{an} is modeled with the following expression

$$w_{an} = \frac{H_{an\perp}}{M_0} l_X^2 - \frac{H_{an\parallel}}{8M_0^3} (l_X^4 + l_Y^4 + l_Z^4), \quad (11)$$

where $H_{an\parallel}$ is the intrinsic anisotropy field within the film plane and the small out-of-plane anisotropy field $H_{an\perp} \ll H_{an\parallel}$ is responsible for weak tetragonality of the sample.

In the absence of field and current a single AFM layer has two equivalent equilibrium orientations of AFM vector (see Fig. 2a, b): $\mathbf{l} \parallel Z$ and $\mathbf{l} \parallel Y$ (as can be easily obtained from minimization of the magnetic energy (11)). Correspondingly, a FM/AFM bilayer has two stable configurations²⁵ with $\mathbf{l} \parallel \mathbf{p}_{cur}$ (Fig. 2a) and with $\mathbf{l} \perp \mathbf{p}_{cur}$ (Fig. 2b). These two configurations should have different macroscopic properties (e.g., different magnetoresistance, different exchange bias field, etc.) and in

this sense are analogous to the parallel (P) and antiparallel (AP) configurations of FM/FM multilayers (Fig. 2 c,d). In analogy with FM/FM systems, the reversible switching between the $\mathbf{l} \parallel \mathbf{p}_{cur}$ and $\mathbf{l} \perp \mathbf{p}_{cur}$ states can be achieved by application of the external magnetic field to the free (in our case, AFM) layer.

The switching field should be oriented parallel to AFM vector, its critical value coincides with the spin-flop transition field $H_{s-f} = 2\sqrt{H_{an\parallel}H_E}$ for AFM layer (also exchange enhanced).

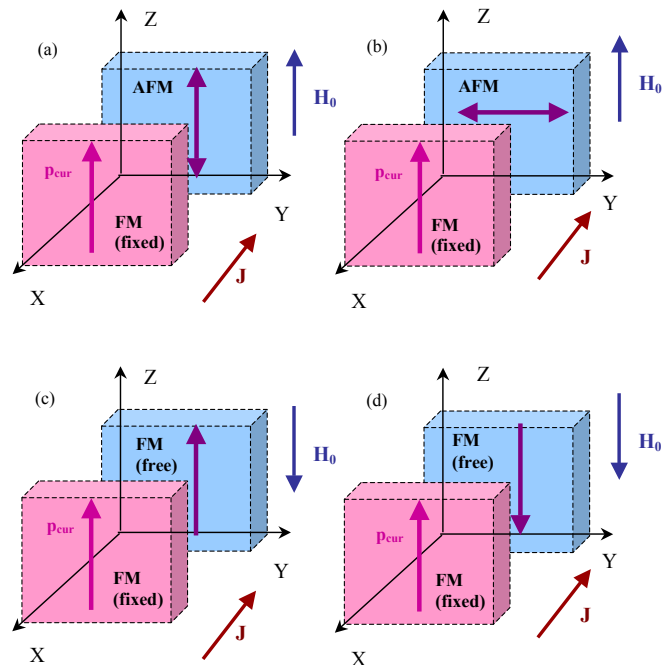


Figure 2. (Color online) **Stable magnetic configurations with different macroscopic properties.** In FM/AFM bilayer (a,b) the magnetization ($\parallel \mathbf{p}_{cur}$) of FM layer is fixed, AFM vector can be switched from (a) parallel to (b) perpendicular orientation with respect to \mathbf{p}_{cur} by application of the external magnetic field $H_0 \geq H_{s-f}$ within an AFM layer. In FM/FM bilayer (c,d) the magnetization of free layer can be switched from (c) parallel to (d) antiparallel orientation with respect to \mathbf{p}_{cur} by the external magnetic field \mathbf{H}_0 applied antiparallel to \mathbf{p}_{cur} . In both cases (c) and (d) the switching can be also induced by current.

When the current is injected into bilayer, configuration with $\mathbf{p}_{cur} \parallel \mathbf{l}$ is still equilibrium, but not necessarily stable. To find the values of critical current and field, we analyze the frequencies of eigen modes of AFM layer (magnetization of FM layer \mathbf{p}_{cur} and, correspondingly, the current polarization being fixed).

A. Configuration $\mathbf{H}_0 \perp \mathbf{l}$

In the crossed initial orientation $\mathbf{H}_0 \perp \mathbf{l}$ (Fig. 1c) the linearized equations of motion for the generalized coordinates l_X, l_Y ($l_Z \approx 2M_0 - (l_X^2 + l_Y^2)/2$) take the following

form:

$$\begin{aligned} \dot{l}_X + 2\gamma_{\text{AFM}}\dot{l}_X + (\omega_X^2 + \omega_H^2)l_X + \gamma H_E \sigma J l_Y &= 0, \\ \dot{l}_Y + 2\gamma_{\text{AFM}}\dot{l}_Y + \omega_Y^2 l_Y - \gamma H_E \sigma J l_X &= 0, \end{aligned} \quad (12)$$

Here $\gamma_{\text{AFM}} \equiv \gamma H_E \alpha_G / 2 \ll \omega_{X,Y}$ is a damping coefficient that can be estimated from the line-width of AFM resonance, $\omega_H = \gamma H_0$. The values $\omega_X = 2\gamma\sqrt{(H_{\text{an}\perp} + H_{\text{an}\parallel})H_E}$, $\omega_Y = 2\gamma\sqrt{H_{\text{an}\parallel}H_E}$ are the eigen frequencies of free oscillations in the absence of field and current that also could be measured in AFM resonance experiments. It is worth noting that the values of eigen frequencies are enhanced due to exchange coupling (multiple H_E) compared to analogous values in FM with the same value of anisotropy field.

Equations (12) describe the case when the magnetic field is directed along the hard anisotropy axis, $\mathbf{H}_0 \parallel X$. Configuration with $\mathbf{H}_0 \parallel Y$ (field is parallel to an easy axis) is treated in an analogous way.

It can be easily seen from (12) that below the critical current

$$|J| \leq J_{\text{cr}}^{(1)} \equiv \frac{1}{2\gamma H_E \sigma} |\omega_X^2 - \omega_Y^2 + \omega_H^2|. \quad (13)$$

the eigen modes have linear polarization and correspond to oscillations of vector \mathbf{l} within XZ or YZ plane (Fig. 1c). In this case the spin torque transferred from the current affects the eigen frequencies of spin excitations,

$$\begin{aligned} \Omega_{\pm}^2 &= \frac{1}{2} [\omega_X^2 + \omega_Y^2 + \omega_H^2 \\ &\pm |\omega_X^2 - \omega_Y^2 + \omega_H^2| \sqrt{1 - \left(\frac{J}{J_{\text{cr}}^{(1)}}\right)^2}], \end{aligned} \quad (14)$$

but does not affect the effective damping coefficients (as it is the case in FM).

It should be stressed that in the absence of external field the value of critical current depends upon anisotropy

$(\omega_X^2 - \omega_Y^2) \propto H_{\text{an}\perp}$ of the magnetic interactions within and perpendicular to the film plane. The magnetic field applied perpendicular to the vector \mathbf{l} enhances (if \mathbf{H}_0 is parallel to an easy axis) or weakens (if \mathbf{H}_0 is parallel to a hard magnetic axis of AFM) the effective anisotropy. So, magnetic field can be used for control of the critical current. If anisotropy is weak ($H_{\text{an}\perp} \ll H_{\text{an}\parallel}$, or, equivalently, $|\omega_X - \omega_Y| \ll \omega_Y$), it can be effectively reduced with the field whose value is much less than the spin-flop one, $H_0 \ll H_{\text{s-f}}$.

Above the critical current, $|J| \geq J_{\text{cr}}^{(1)}$, polarization of free oscillations changes from linear to circular (elliptic) and STT contributes into the energy dissipation. For one of two modes of free oscillations the current-induced pumping competes with the internal damping. Starting from the critical value

$$J_{\text{cr}}^{(2)} \equiv \sqrt{(J_{\text{cr}}^{(1)})^2 + \frac{2\gamma_{\text{AFM}}^2}{\gamma^2 H_E^2 \sigma^2} (\omega_X^2 + \omega_Y^2 + \omega_H^2)}, \quad (15)$$

the average energy losses per oscillation period are negative (pumping is greater than damping) and the state with the parallel alignment of current polarization and AFM vector becomes unstable.

As seen from Eq.(15), the value of critical current $J_{\text{cr}}^{(2)}$ is independent on the directions of current, field and spin polarization (\mathbf{p}_{curr}), in contrast to the threshold current for FM.

B. Configuration $\mathbf{H}_0 \parallel \mathbf{l}$

Another type of dynamics is observed in the case when the field is applied parallel to \mathbf{l} (Fig. 1d). In this case polarization of eigen modes is circular (or elliptic) even for $J = 0$, as follows from symmetry considerations and from analysis of equations of motion written in terms of appropriate generalized coordinates $l_{\pm} = l_X \pm i l_Y$:

$$\ddot{l}_{\pm} + 2(\gamma_{\text{AFM}} \mp i\omega_H) \dot{l}_{\pm} + \left[\frac{1}{2}(\omega_X^2 + \omega_Y^2) - \omega_H^2 \mp i\gamma H_E \sigma J \right] l_{\pm} + \frac{1}{2}(\omega_X^2 - \omega_Y^2) l_{\mp} = 0. \quad (16)$$

So, oscillations of \mathbf{l} can actively take up an energy from the current and STT affects the damping coefficient, not the frequency of oscillations. Instability point is attained as soon as the spin-polarized current overcomes the effect of internal friction.

Fig. 3a) shows the field-current stability diagram for the case of isotropic AFM ($H_{\text{an}\perp} = 0$ and, correspondingly, $\omega_X = \omega_Y$). Within the shaded area

$$\left| J - \frac{2\gamma_{\text{AFM}} H_0}{\sigma H_E} \right| \leq \frac{2\gamma_{\text{AFM}} H_{\text{s-f}}}{\sigma H_E}, \quad |H_0| \leq H_{\text{s-f}}, \quad (17)$$

the static state with $\mathbf{l} \parallel \mathbf{p}_{\text{curr}} \parallel Z$ is stable. Above the critical value, $|J| \geq |J_{\text{cr}}|$, where

$$J_{\text{cr}} \equiv \frac{2\gamma_{\text{AFM}}}{\sigma H_E} (H_0 + H_{\text{s-f}} \text{sign} J), \quad (18)$$

the current may keep up a stable rotation of AFM vector around \mathbf{p}_{curr} (Fig. 3b). Sign reversal of STT (resulted from the reversal of either direction of current, $J \rightarrow -J$, or direction of polarization, $\mathbf{p}_{\text{curr}} \rightarrow -\mathbf{p}_{\text{curr}}$) gives rise to rotation in opposite direction. If the field value is greater

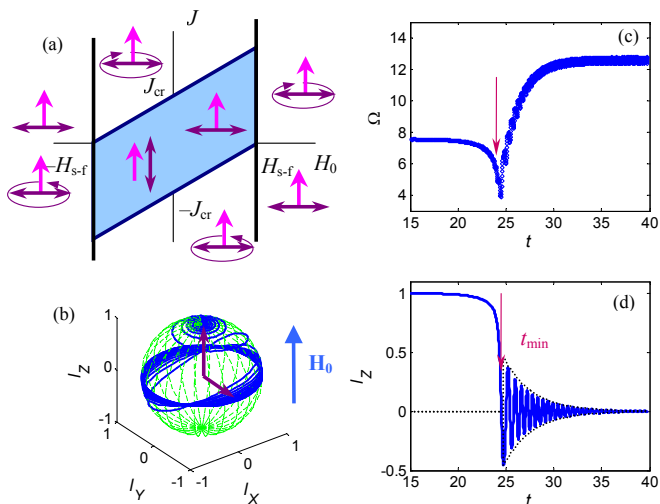


Figure 3. (Color online) **Dynamics of AFM vector induced by steady spin-polarized current.** (a) Stability diagram under combined action of field and current. Static states of the bilayer (schematically shown with an arrow for \mathbf{p}_{cur} and double arrow for AFM vector) are stable within the shaded area. Strong current ($|J| > J_{\text{cr}}$) induces precession of an AFM vector around the current polarization \mathbf{p}_{cur} , direction of rotation depends on the sign of J . Strong field ($|H_0| > H_{s-f}$) induces spin-flop transition combined with the current-induced precession. (b) 3-D evolution of AFM vector \mathbf{l} in overcritical regime ($J > J_{\text{cr}}$) in the presence of magnetic field \mathbf{H}_0 . In the initial state the AFM vector is slightly misaligned from Z axis. Under the action of STT the vector \mathbf{l} spirals away from Z axis with a steadily-increasing precession angle and the angular frequency Ω . Final state corresponds to precession with the stable frequency within XY plane ($l_z = 0$). (c), (d) Time dependence of the angular frequency Ω and l_z projection. Arrows indicate the moment, t_{min} , at which monotonic decrease of l_z switches to the decaying oscillations. Envelope (dash line) corresponds to relaxation ($\propto \exp(-\gamma_{\text{AFM}}t)$) caused by internal damping.

than spin-flop field, $|H_0| \geq H_{s-f}$, the state with $\mathbf{l} \parallel \mathbf{H}_0$ is unstable even in the absence of current and in the final state the AFM vector is perpendicular to \mathbf{H}_0 and \mathbf{p}_{cur} . These results also keep true for small but nonzero anisotropy $H_{\text{an}\perp}$.

The current-induced precession of \mathbf{l} vector is also stable in the “high-field” region, $|H_0| \geq H_{s-f}$. However, detailed analysis of the dynamical phases and transition lines in this region is out of scope of this paper.

Some features of the current-induced instability in configuration with $\mathbf{l} \parallel \mathbf{H}_0$ are similar to those observed in FM/FM bilayers. First, in both cases the stability region is defined by an internal friction which stands up against the current-induced rotations²⁶. Second, the value of critical current linearly depends on the field^{12,27}. Thus, application of the magnetic field results in variation of the critical current and opens a possibility to reduce J_{cr} , as seen from Fig. 3a.

On the other hand, there are still few principal differences between FM/FM and FM/AFM bilayers listed

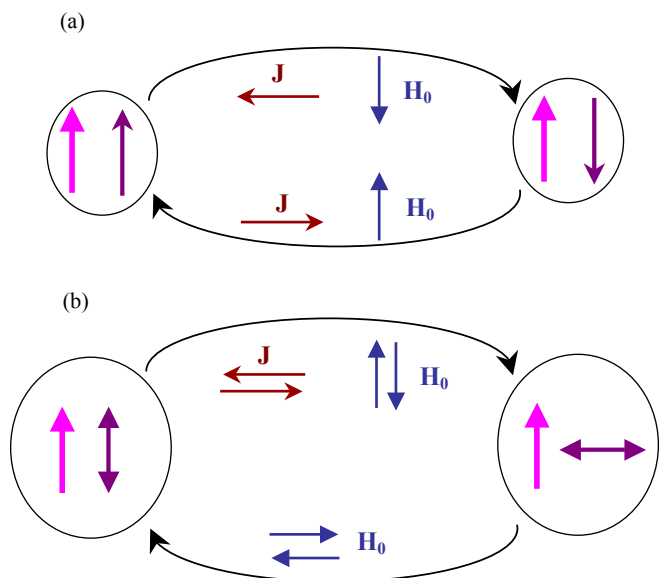


Figure 4. (Color online) **Switching between the different configurations of FM/FM (a) and FM/AFM (b) bilayers.** Magnetization of the fixed layer is shown with magenta (thick) arrow, that of the free layer with violet (thin arrow), double arrow shows orientation of AFM vector. (a) Switching between P and AP states can be achieved by the field or current applied in two opposite directions. (b) Transition from parallel to perpendicular configuration can be induced by current (arbitrary direction) and field applied along initial orientation of AFM vector. Transition from perpendicular to parallel configuration can be induced by the field only.

below.

- In the FM/FM bilayer (one FM layer being fixed) switching between P and AP states can be achieved by application of *either* field or current (Fig. 4a). In contrast, in the FM/AFM bilayer switching between $\mathbf{l} \parallel \mathbf{p}_{\text{cur}}$ and $\mathbf{l} \perp \mathbf{p}_{\text{cur}}$ states can be achieved by a *combined* application of field and current (Fig. 4b). Namely, the current induces transition only from $\mathbf{l} \parallel \mathbf{p}_{\text{cur}}$ to $\mathbf{l} \perp \mathbf{p}_{\text{cur}}$ because the last state is stable in the presence of current. To reverse \mathbf{l} vector back to $\mathbf{l} \parallel \mathbf{p}_{\text{cur}}$ configuration, one needs to apply an external field $H_0 \geq H_{s-f}$ parallel to \mathbf{l} (spin-flop transition).
- In the FM/FM bilayer the direction of current (from fixed to free layer or opposite) is important, $P \rightarrow AP$ and $AP \rightarrow P$ transitions take place at opposite directions of current (Fig. 4a). In contrast, in the FM/AFM bilayer destabilization of $\mathbf{l} \parallel \mathbf{p}_{\text{cur}}$ state takes place irrespective of the current direction (Fig. 4b). However, an external magnetic field removes such a degeneracy.
- The bilayers with AFM should show exchange reduction of the critical current compared to FM/FM

bilayers providing that the free FM and AFM layers have the same magnetic resonance frequencies (or anisotropy field of FM is close to spin-flop field of AFM) and the same quality factor ($=\omega/\gamma_{\text{AFM}}$), as can be seen from Eq. (18).

VI. DYNAMICS IN OVERCRITICAL REGIME

A FM layer subjected to the direct spin-polarized current shows one interesting effect – stable precession of

$$\begin{aligned} \ddot{\theta} + 2\gamma_{\text{AFM}}\dot{\theta} + \sin\theta\cos\theta \left[\omega_Y^2 - (\dot{\varphi} - \omega_H)^2 + \frac{\omega_X^2 - \omega_Y^2}{2}(1 + \cos 2\varphi) - \frac{\omega_Y^2 - \omega_H^2}{4}\sin^2\theta(7 + \cos 4\varphi) \right] &= 0, \\ \frac{d}{dt} [(\dot{\varphi} - \omega_H)\sin^2\theta] + \sin^2\theta \left[2\gamma_{\text{AFM}}\dot{\varphi} - \gamma H_E J\sigma + \frac{\omega_Y^2 - \omega_X^2}{2}\sin 2\varphi + \frac{\omega_Y^2 - \omega_H^2}{4}\sin^2\theta\sin 4\varphi \right] &= 0. \end{aligned} \quad (19)$$

As it was already mentioned, an AFM under consideration is an oscillator with the high quality factor ($\omega_{X,Y} \gg \gamma_{\text{AFM}}$). In other words, energy dissipation takes place on the time scale much greater than the characteristic period of free oscillations. In this case for analytical treatment of Eqs. (19) one can apply the asymptotic method of rapidly rotating phase originated by Bogolyubov and Mitropolskii²⁸.

According to this method, the motion of AFM vector is decomposed into rapid rotation with the frequency $\Omega \propto \omega_{X,Y}$ and slow variation of amplitude and frequency with the characteristic time scale $\propto 1/\gamma_{\text{AFM}}$. In the simplest case of isotropic AFM ($H_{\text{an}\perp} = 0$, or $\omega_X = \omega_Y$) the only rapid variable is $\varphi = \Omega(t)t$. Equations for slow variables $\Omega(t)$ and $\theta(t)$ ($\dot{\Omega}, \dot{\theta} \ll \Omega$) are obtained from (19) by averaging over the period of rotation:

$$\begin{aligned} \ddot{\theta} + 2\gamma_{\text{AFM}}\dot{\theta} \\ + \sin\theta\cos\theta \left[\omega_0^2 - (\Omega - \omega_H)^2 - \frac{7}{4}\omega_0^2\sin^2\theta \right] &= 0, \quad (20) \\ \frac{d}{dt} [(\Omega - \omega_H)\sin^2\theta] + \sin^2\theta (2\gamma_{\text{AFM}}\Omega - \gamma H_E J\sigma) &= 0. \end{aligned}$$

If, in addition, $\dot{\Omega} \ll \dot{\theta}$, the first of equations (20) describes 1D motion (dynamic variable θ) in a potential well (see Fig. 5)

$$U(\theta; \Omega) = \frac{1}{2}\sin^2\theta \left[\omega_0^2 - (\Omega - \omega_H)^2 - \frac{7}{4}\omega_0^2\sin^2\theta \right], \quad (21)$$

with the friction defined by coefficient γ_{AFM} . The second of Eqs. (20) describes the current-induced variation of both variables θ and Ω .

Equations (20) have two interesting solutions. The first one, corresponds to the circular polarized free oscillations of AFM vector with an amplitude $\theta = \theta_0 \ll 1$ and eigen frequency $\Omega_0 \equiv \omega_X + \omega_H$. However, in overcritical regime

magnetization with the angular frequency close to the frequency of spin-wave mode^{4,5}. To find out whether such an effect could be observed in AFM, we consider in details the dynamics of AFM vector in overcritical regime ($|J| > |J_{\text{cr}}|$) assuming that $\mathbf{p}_{\text{cur}} \parallel \mathbf{H}_0 \parallel Z$.

We use the standard parametrization of AFM vector with the spherical angles θ and φ , $l_X = 2M_0 \sin\theta \cos\varphi$, $l_Y = 2M_0 \sin\theta \sin\varphi$, $l_Z = 2M_0 \cos\theta$, to deduce the following dynamic equations:

an amplitude θ_0 growth with an increment proportional to the offset from the critical current value:

$$\frac{1}{\tau} \equiv \gamma_{\text{AFM}} \left| \frac{J - J_{\text{cr}}}{J_{\text{cr}}} \right| \left(1 + \frac{H_0}{H_{\text{s-f}}} \right). \quad (22)$$

The second solution with $\theta = \pi/2$ corresponds to steady rotation of AFM vector in XY plane ($l_Z = 0$) with the angular frequency $\Omega_\infty = (J/J_{\text{cr}})\Omega_0$. Energy dissipation per period of rotation is zero, due to the pretty balance between the magnetic damping and current-induced pumping. This solution is stable when $|J| > |J_{\text{cr}}|$, as can be seen from analysis of the potential $U(\theta; \Omega)$. Small deviations of AFM vectors from XY plane ($|\theta - \pi/2| \ll 1$) relax due to internal friction as

$$\cos\theta \propto e^{-\gamma_{\text{AFM}}t} \cos(\Omega_\infty t + \psi), \quad (23)$$

where ψ is a phase that depends upon initial conditions and

$$\Omega_\theta = \sqrt{\Omega_\infty^2 - 2\Omega_\infty\omega_H + \frac{3}{4}(\omega_0^2 - \omega_H^2)}. \quad (24)$$

So, the state of steady precession is approached during the time $1/\gamma_{\text{AFM}}$ that depends upon the internal magnetic damping.

To illustrate all the described peculiarities of AFM dynamics in the presence of spin-polarized current we solve the original Eqs. (19) numerically with the initial conditions $\theta = \theta_0 = 0.001$, $\varphi = \pi/2$, $\dot{\theta} = 0$ and $\dot{\varphi} = \Omega_0$. In other words, at $t = 0$ an AFM vector deflects from equilibrium orientation $\mathbf{l} \parallel Z$ through the small angle $\theta_0 \ll 1$ within the ZY plane. Initial velocity corresponds to that mode of free oscillations which is unstable for the chosen current direction. For calculations we used the following dimensionless values: $\omega_X = \omega_Y = 6.28$ and $\gamma_{\text{AFM}} = 0.314$ (that corresponds to the quality factor

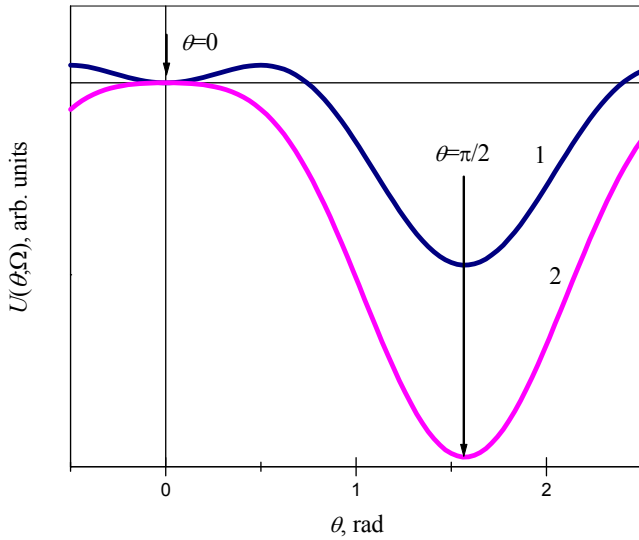


Figure 5. Profile of the effective potential well (21), arbitrary units. 1 – $\Omega \leq \Omega_0$, 2 – $\Omega > \Omega_0$. Arrows indicate static solution ($\theta = 0$) unstable in overcritical regime and stable stationary solution ($\theta = \pi/2$).

20). Time unit equals to the period of free oscillations in the absence of field and current.

Fig. 3b shows a typical trajectory of AFM vector (normalized to a unit length) in the presence of steady current $J = 2.5J_{cr} < 0$ and field $H = 0.2H_{sf}$. With the described initial conditions, the motion of \mathbf{l} vector starts as a rotation around Z axis with the eigen frequency Ω_0 of free oscillations. Due to the energy pumping from STT, an amplitude of oscillations (\mathbf{l} projection on XY plane) slowly increases with an increment τ (see Eq. (22)).

The final state ($t \rightarrow \infty$) corresponds to the above described steady rotation of AFM vector in XY plane ($l_Z = 0$) with the angular frequency Ω_∞ . In analogy with FM, such a precessional state of an AFM layer can be a source of spin waves. In contrast to FM, the angular frequency Ω_∞ is proportional to the current value. The absolute value of Ω_∞ is greater than the characteristic spin-wave frequency ($\propto \Omega_0$) which in AFM can range THz values (e.g., for bulk FeMn the energy gap is 7 meV²⁹ that corresponds to linear frequency $\propto 2$ THz). So, FM/AFM bilayer can be considered as a potential emitter of high frequency spin waves.

Figs. 3c and 3d illustrate the time evolution of the rotation frequency Ω and the component l_Z between the initial and final states. Due to nonlinear effects, deflection of \mathbf{l} from the initial direction is accompanied by decrease of Ω . At a certain moment $t = t_{min}$ (shown by arrow in Figs. 3 c,d) a monotonic decrease of l_Z changes into decaying oscillations around the average value $l_Z = 0$. Relaxation of \mathbf{l} to XY plane is due to internal damping and follows the law $\propto \exp(-\gamma_{AFM}t)$ (see Eq. (23) and envelope in Fig. 3d). The details of relaxation to the precessional state are shown in Fig. 6 where we compare an exact solution (points) of (19) with the asymptotic form

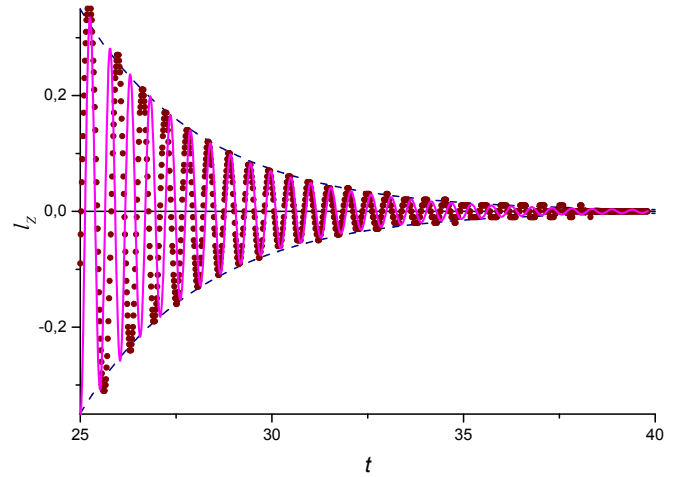


Figure 6. (Color online) Relaxation dynamics of slow amplitude l_Z at $t \geq t_{min}$. Points – numerical simulation, solid line – approximation according to Eq. (23), dashed line – envelope $\propto \exp(-\gamma_{AFM}t)$.

(solid line) calculated from the expressions (22), (23).

In our simulations of AFM dynamics we found that not only l_Z , but the rotation frequency Ω , energy dissipation rate and the effective potential energy averaged over a period of rotation ($= 2\pi/\Omega$) has an extremum at the moment $t = t_{min}$. This means that the system passes through the crossing between two attraction points in the phase space. So, we interpret the time interval t_{min} as a switching time between two stable states of the FM/AFM bilayer (see Figs. 2 a,b, and 4 b). The exact value of

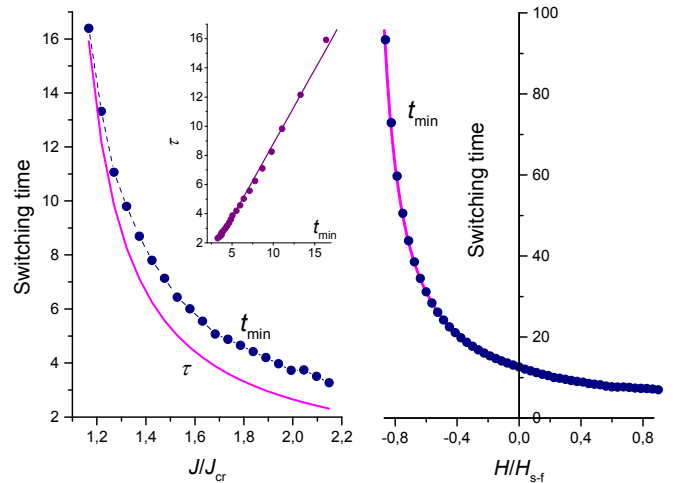


Figure 7. (Color online) **Switching time from parallel to perpendicular configurations shown in Fig. 2 a,b.** (a) Current dependence of the calculated switching time, t_{min} , and the effective pumping coefficient $\tau \propto |J - J_{cr}|^{-1}$, external magnetic field $H_0 = 0.2H_{sf}$ is parallel to Z . Inset shows correlation between τ and t_{min} . (b) Field dependence of switching time t_{min} at fixed bias current (points). Solid line shows approximation $\propto |H_{sf} + H_0|^{-1}$.

t_{\min} depends upon the initial deflection θ_0 of AFM vector from Z axis (or, in other words, from the amplitude of spontaneous fluctuations and, hence, from temperature). However, the current and field behaviour of t_{\min} is the same for different initial conditions and correlates with the current (Fig. 7a) and field (Fig. 7b) behavior of the characteristic time τ of destabilization (22). Though the absolute values of t_{\min} and τ are different, they show good correlation (see inset in Fig. 7a) in rather wide range of current values. Both values decrease moving far from the stability point J_{cr} . This opens a way to diminish the switching time by increasing the current value or by decreasing the critical current with the magnetic field.

VII. CONTROLABLE SWITCHING OF AFM STATE

From practical point of view it is important to achieve a controllable switching between the different equilibrium states of the FM/AFM bilayer (say, $\mathbf{l} \parallel \mathbf{p}_{\text{cur}} \rightarrow \mathbf{l} \perp \mathbf{p}_{\text{cur}}$ or $\mathbf{l} \parallel -\mathbf{p}_{\text{cur}}$) using the current pulses of minimal duration and amplitude. We investigate dynamics of AFM vector under the rectangular current pulses (schematically shown by red line in Fig. 8) of different duration and amplitude in overcritical regime ($|J| > |J_{\text{cr}}|$). If pulse duration is below t_{\min} , AFM vector returns back to its initial state after the current is switched off.

Fig. 8 demonstrates the switching processes initiated by the current pulse $J = 2.5J_{\text{cr}}$ with the duration slightly greater than t_{\min} . The chosen pulse duration ensures maximum deflection of AFM vector from the initial direction as seen from time dependence of l_Z (Fig. 8 a). After the current is switched off, the AFM vector relaxes to the final static state within XY plane through the damping oscillations during the time $1/\gamma_{\text{AFM}}$. Regular rotation around Z axis supported by current also vanishes with the end of current pulse, as seen from Ω behaviour (Fig. 8b). The final orientation of AFM vector is parallel to one of the easy axes within XY plane (in the presence of field, Fig. 8c) or can be also antiparallel to the initial \mathbf{l} direction (180° switching to Z easy axis) in the absence of external field (Fig. 8d). Due to degeneracy, the final state is very sensitive to the initial conditions and pulse duration and can be predicted only statistically.

VIII. CONCLUSIONS

In summary, we studied the dynamics of AFM layer in the presence of spin-polarized current and external magnetic field.

On the basis of a simple model of slightly tetragonal AFM with two magnetic sublattices we demonstrated the following features of current-induced behavior in the FM/AFM bilayer.

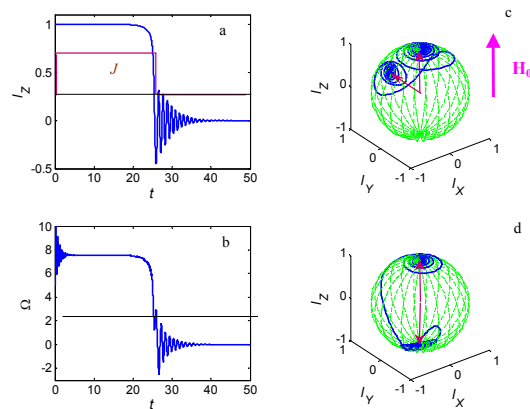


Figure 8. (Color online) **Dynamics of AFM vector induced by a pulse of spin-polarized current.** (a) Time dependence of l_Z (thick or blue line) under the rectangular current pulse (thin or red line). Pulse duration close to t_{\min} is enough to ensure maximal deflection of l_Z from the initial value. (b) High frequency rotation of AFM vector persists as long as current induces STT, as seen from time dependence of Ω . Just after the current is switched off the frequency of rotation goes down to zero and AFM vector lies down to XY plane. Relaxation time ($= 1/\gamma_{\text{AFM}}$) of both Ω and l_Z is due to internal damping. (c) Magnetic field applied parallel to the initial orientation of \mathbf{l} induces 90° switching, the final state of AFM vector is parallel to XY plane. (d) In isotropic AFM in the absence of field a spin-polarized current may induce 180° switching.

1. Spin transfer torque induces the loss of stability in the FM/AFM system if AFM vector is parallel to FM magnetization. Configuration with AFM vector perpendicular to FM magnetization is stable in the presence of current and field (in accordance with the prediction made in Ref.17). This means that the high density current can induce reorientation of AFM vector if an angle between \mathbf{l} and \mathbf{p}_{cur} differs from $\pi/2$.
2. Such a current can also induce a stable precession of AFM vector in the plane perpendicular to FM magnetization. The frequency of precession is of the order of frequency of free oscillations and linearly depends on current.
3. The value of critical current can be tuned by application of the external magnetic field. The value of switching time can be tuned by both field and current.

We anticipate the same features in noncollinear AFM with three (like IrMn_3 and Mn_3NiN) and more (like FeMn) magnetic sublattices.

On the other hand, our model predicts irreversible current-induced switching between the parallel and perpendicular orientations of \mathbf{l} and \mathbf{p}_{cur} . This result is the consequence of the chosen tetragonal magnetic anisotropy. In the case when an angle between easy axes of AFM differs from $\pi/2$ (like in NiO or FeMn),

the current-induced switching seems to be possible between all the configurations of \mathbf{l} and \mathbf{p}_{cur} as long as \mathbf{l} has a nonzero projection on \mathbf{p}_{cur} .

The described response of AFM vector to electron current may change the properties of the pinned layer. Due to the weak but nonzero exchange coupling between AFM and FM layers, reorientation or precession of AFM vector results in variation of the exchange bias field and, consequently, gives rise to the shift of switching fields of spin-valve. We illustrate this effect qualitatively in Fig. 9. Consider a typical spin-valve with the pinned FM layer. Suppose, an AFM layer is inhomogeneous (multidomain) and high density current gives rise to reorientation of AFM vector in some of domains (Fig. 9a). The ratio of the rotated domains is proportional to the integral current. On the other hand, reorientation of some AFM domains results in diminishing of the exchange bias field that keeps FM magnetization of the pinned layer. Variation of the bias field is also proportional to the ratio of the rotated AFM domains. So, in the presence of current the critical field at which magnetization of the pinned layer is reversed decreases linearly. However, linear shift of the bias field can be also induced by STT between FM layers. If AFM layer is not affected by spin transfer torque, the stability region of AP configuration increases for one current direction and diminishes for an opposite, as shown in Fig. 9b. On the contrary, if spin torque is transferred to an AFM layer and is not transferred between two FM layers, the stability region of antiparallel configuration of FM layers diminishes for any current direction (Fig. 9c). The last type of current dependence (among others) was observed in the experiments Ref.14. Decrease of the exchange bias field irrespective of current direction was also observed in Ref.9.

Linear shift of the bias field induced by the current was observed in nanopillars⁷ that included coupled permalloy (FM) and FeMn (AFM) layers. In these experiments a combined application of the magnetic field and high-density current resulted in an increase of the exchange bias field from -100 to 100 Oe.

Another evidence of STT effects in AFM could be found from the detailed analysis of the field/current dependence of magnetoresistance, as it was done in Refs.6, 8–10. Magnetoresistance of spin valve should depend on the angle between FM and AFM vectors (in addition to the dependence from mutual orientation of FM vectors in “free” and “pinned” layers) and can change due to the current-induced switching of AFM vector.

Appendix A: Relation between magnetization and AFM vector

Small macroscopic magnetization $|\mathbf{m}| \ll |\mathbf{l}|$ of AFM layer can be excluded from Eq.(5) in the following way^{24,30}. Free energy of AFM layer is modeled as

$$w = \frac{H_E}{4M_0} \mathbf{m}^2 + w_{\text{an}} - \mathbf{H}_0 \mathbf{m}, \quad (\text{A. 1})$$

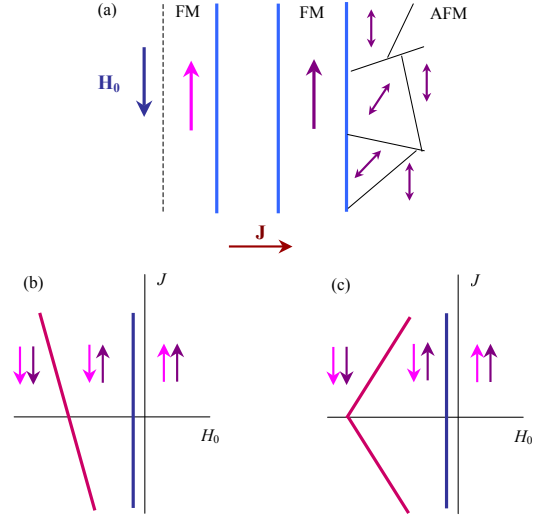


Figure 9. (Color online) **Current dependence of the exchange bias field.** (a) Exchange bias spin-valve structure with multidomain AFM layer. AFM vector in some of domains deflects from the initial orientation due to STT. (b) The shift of bias for typical spin transfer (AFM layer is not affected by current). (c) The shift of bias in the case when spin torque is transferred to AFM layer.

where H_E is the spin-flip field of the exchange nature, w_{an} is anisotropy energy, \mathbf{H}_0 is external magnetic field. In assumption that $H_E M_0 \gg w_{\text{an}}$ (or, equivalently, $H_E \gg H_L$) and $H_E \gg H_0$ (strong exchange coupling), the effective magnetic field is expressed as follows:

$$\mathbf{H}_M \equiv -\frac{\partial w}{\partial \mathbf{m}} = \mathbf{H}_0 - \frac{H_E}{2M_0} \mathbf{m}. \quad (\text{A. 2})$$

We substitute (A. 2) into (5), neglect dissipative terms (with α_G and J) and get

$$\dot{\mathbf{l}} = \gamma \left([\mathbf{H}_0 \times \mathbf{l}] - \frac{H_E}{2M_0} [\mathbf{m} \times \mathbf{l}] \right). \quad (\text{A. 3})$$

To obtain an explicit expression (6) for \mathbf{m} we multiply both sides of Eq.(A. 3) by the vector \mathbf{l} and take into account that $[\mathbf{l} \times [\mathbf{m} \times \mathbf{l}]] = \mathbf{m} \mathbf{l}^2 \approx 4M_0^2 \mathbf{m}$. The last relation follows from the fact that below the Néel temperature both vectors \mathbf{l} and \mathbf{m} are bound by the constraint $\mathbf{l}^2 + \mathbf{m}^2 = 4M_0^2$, $(\mathbf{l}, \mathbf{m}) = 0$ (that is equivalent to the requirement $|\mathbf{M}_1| = |\mathbf{M}_2| = M_0$).

Appendix B: Lagrange and Rayleigh functions for antiferromagnet

The Lagrange function (8) and the Rayleigh function (9) are selected in such a way that to fulfill the following requirements:

- i) The dynamic Eqs.(7) are the Euler-Lagrange equa-

tions of the second kind with dissipative forces:

$$\begin{aligned} & \left[\frac{d}{dt} \frac{\partial \mathcal{L}_{\text{AFM}}}{\partial \dot{\mathbf{l}}} \times \mathbf{l} \right] - \left[\frac{\partial \mathcal{L}_{\text{AFM}}}{\partial \mathbf{l}} \times \mathbf{l} \right] \\ & = - \left[\frac{\partial \mathcal{R}_{\text{AFM}}}{\partial \dot{\mathbf{l}}} \times \mathbf{l} \right]. \end{aligned} \quad (\text{A. 1})$$

- ii) The effective potential energy in Lagrange function coincides with the magnetic anisotropy energy (11).
- iii) Rayleigh function is related with the rate of energy

losses (3) according to Eq.(10).

Expression for energy losses is obtained from (3) by substitution $\mathbf{M}_1 = -\mathbf{M}_2 = \mathbf{l}/2$. Contribution from \mathbf{m} -depending terms into Rayleigh function is small and so, is neglected.

Lagrange approach makes it possible to account for the constraint $|\mathbf{l}| = 2M_0$ (valid far below the Néel point) by appropriate choice of two generalized coordinates q_k ($k = 1, 2$) instead of three components of vector \mathbf{l} , as described in the paper.

-
- ¹ L. Berger, *Phys. Rev. B* **54**, 9353 (1996)
 - ² J. C. Slonczewski, *Phys. Rev. B* **39**, 6995 (1989) .
 - ³ J. Slonczewski, *J. Mag. Mag. Mater.* **159**, L1 (1996).
 - ⁴ S. Kaka, M. R. Pufall, W. H. Rippard, T. J. Silva, S. E. Russek, and J. A. Katine, *Nature* **437**, 389 (2005).
 - ⁵ A. Slavin and V. Tiberkevich, *IEEE Trans. Magn.* **45**, 1875 (2009)
 - ⁶ Z. Wei, A. Sharma, A. S. Nunez, P. M. Haney, R. A. Duine, J. Bass, A. H. MacDonald, and M. Tsoi, *Phys. Rev. Lett.* **98**, 116603 (2007).
 - ⁷ S. Urazhdin and N. Anthony, *Phys. Rev. Lett.* **99**, 046602 (2007)
 - ⁸ X.-L. Tang, H.-W. Zhang, H. Su, Z.-Y. Zhong, and Y.-L. Jing, *Appl. Phys. Lett.* **91**, 122504 (2007)
 - ⁹ N. V. Dai, N. C. Thuan, L. V. Hong, N. X. Phuc, Y. P. Lee, S. A. Wolf, and D. N. H. Nam, *Phys. Rev. B* **77**, 132406 (2008) .
 - ¹⁰ J. Bass, A. Sharma, Z. Wei, and M. Tsoi, *Jour. of Magnetism (Korean Magnetism Society)* **13**, 1 (2008)
 - ¹¹ M. Tsoi, A. G. M. Jansen, J. Bass, W.-C. Chiang, M. Seck, V. Tsoi, and P. Wyder, *Phys. Rev. Lett.* **80**, 4281 (1998).
 - ¹² J. Grollier, V. Cros, H. Jaffrès, A. Hamzic, J. M. George, G. Faini, J. Ben Youssef, H. Le Gall, and A. Fert, *Phys. Rev. B* **67**, 174402 (2003)
 - ¹³ D. C. Ralph and M. D. Stiles, *J. Mag. Mag. Mater.* **320**, 1190 (2008)
 - ¹⁴ J. Basset, A. Sharma, Z. Wei, J. Bass, and M. Tsoi, *Proc. of SPIE, Spintronics* **7036**, 703605 (2008) .
 - ¹⁵ Y. Tserkovnyak, H. J. Skadsem, A. Brataas, and G. E. W. Bauer, *Phys. Rev. B* **74**, 144405 (2006)
 - ¹⁶ A. Nunez, R. Duine, P. Haney, and A. MacDonald, *Phys. Rev. B* **73**, 214426 (2006).
 - ¹⁷ P. M. Haney and A. H. MacDonald, *Phys. Rev. Lett.* **100**, 196801 (2008) .
 - ¹⁸ Y. Xu, S. Wang, and K. Xia, *Phys. Rev. Lett.* **100**, 226602 (2008)
 - ¹⁹ E. V. Gomonay and V. M. Loktev, *Sov. J. Low Temp. Phys.* **34**, 198 (2008) .
 - ²⁰ P. M. Haney, D. Waldron, R. A. Duine, A. S. N. nez, H. Guo, and A. H. MacDonald, *Phys. Rev. B* **75**, 174428 (2007) .
 - ²¹ P. M. Haney, D. Waldron, R. A. Duine, A. S. N. nez, H. Guo, and A. H. MacDonald, *Phys. Rev. B* **76**, 024404 (2007)
 - ²² V. G. Bar'yakhtar, *Sov. Phys. — JETP* **60**, 863 (1984)
 - ²³ A. I. Akhiezer, V. G. Bar'yakhtar, and S. V. Peletminskii, *Spin Waves*, Interscience (Wiley) ed., North-Holland Series in Low Temperature Physics, Vol. 1 (North-Holland, Amsterdam, 1968).
 - ²⁴ I. Bar'yakhtar and B. Ivanov, *Sov. — J. Low Temp. Phys.* **5**, 361 (1979).
 - ²⁵ In the bilayer structure the orientation of AFM vector is governed by competition between the intrinsic magnetic anisotropy (11) and exchange coupling with the adjacent FM layer. However, in the typical cases an effective field of exchange coupling is much smaller than the spin-flop field of AFM and thus can be neglected.
 - ²⁶ S. I. Kiselev, J. C. Sankey, I. N. Krivorotov, N. C. Emley, R. J. Schoelkopf, R. A. Buhrman, and D. C. Ralph, *Nature* **425**, 380 (2003).
 - ²⁷ Y. V. Gulyaev, P. E. Zil'berman, E. M. Epshtein, and R. J. Elliott, *Sov. Phys.— JETP* **100**, 1005 (2005).
 - ²⁸ N. N. Bogolyubov and Y. A. Mitropolskii, *Asymptotic methods in the theory of nonlinear oscillations* (Taylor and Francis, Inc., 1961) 548 p.
 - ²⁹ Y. Endoh, G. Shirane, Y. Ishikawa, and K. Tajima, *Solid State Commun.* **13**, 1179 (1973).
 - ³⁰ A. V. Kimel, B. A. Ivanov, R. V. Pisarev, P. A. Usachev, A. Kirilyuk, and T. Rasing, *Nature Physics* **5**, 727 (2009)